Influence of Particle Size and Gradation on Liquefaction Potential and Dynamic Response

Alexander P. Pires-Sturm, Ph.D., M.ASCE[1]; and Jason T. DeJong, Ph.D., F.ASCE[2]

Abstract: Centrifuge testing data are presented to elucidate the influence of particle size and gradation on liquefaction potential and dynamic response. The physical, index, and material properties of nine test soil mixtures, sharing a common geologic origin and ranging in D_{50} from 0.18 to 2.58 mm and C_u from 1.53 to 9.86, were quantified and compared to the range of values exhibited by clean sands in the literature. Each centrifuge model was subjected to 15 dynamic loading events across a range of relative density and Arias intensity levels. The high permeability of the poorly graded soils prevented flow liquefaction; however, the gap and well-graded soils generated excess pore pressures similar to clean sands even though large particles were present. Despite similar pore pressure responses, the gap and well-graded test soils exhibited lower cumulative volumetric strains than the clean sand because of enhanced dilation. The tendency for the gap and well-graded soils to dilate is theorized to stem from their enhanced packing efficiency and increased shear stiffness. **DOI: 10.1061/(ASCE)GT.1943-5606.0002799.** © *2022 American Society of Civil Engineers.*

Introduction

Standard of practice assumes that the liquefaction susceptibility of all coarse grained soils can be reasonably evaluated using sand-based methods, such as the triggering curves of Idriss and Boulanger (2008). These triggering curves related penetration resistance to cyclic strength; however, both parameters have been shown to vary with particle size and gradation in coarse-grained soils.

Penetration resistance has been shown to increase with particle size as the particle-to-probe diameter ratio decreases and the continuum failure mechanism becomes compromised (e.g., Bolton et al. 1999; Daniel et al. 2004; Sturm 2019). For example, Sturm (2019) found that cone penetration test (CPT) tip resistance increased by a factor of 2.5 when the mean particle diameter (D_{50}) increased from 0.18 to 2.58 mm (all else being equal). This effect can be circumvented in practice by applying corrections to the measured penetration resistance (e.g., Idriss and Boulanger 2008) or by using large-scale penetrometers (e.g., DeJong et al. 2017) to keep the probe-to-particle diameter ratio within an acceptable range.

Penetration resistance has also been shown to increase with gradation due to the associated increases in soil stiffness and strength. For example, Sturm (2019) found that CPT tip resistance increased by a factor of 2.4 when the coefficient of uniformity (C_u) increased from 1.68 to 7.44 (all else being equal). Kulhawy and Mayne (1990) and Ghali et al. (2019) proposed methods to systematically account of the effects of gradation on penetration resistance; however, these methods cannot account for the influence of particle crushing, which can become a significant factor at high stresses or for soils composed of weak grains.

Since penetration resistance increases with particle size and gradation, cyclic resistance must also increase proportionally to validate the standard of practice of using clean sand-based liquefaction triggers curved to evaluate all coarse-grained soils. Numerous laboratory and field studies have aimed to understand the effects of particle size and gradation on cyclic strength; however, most have included gravel-sized particles to achieve a broader range of D_{50} and C_u values. Fundamentally, there is nothing significant about the particle size threshold between sand and gravel particles, as evidenced by the discrepancies between major classification systems (4.75 mm for unified soil classification system (USCS) and 2.0 mm for the Japanese, British, and German classification systems). All coarse-grained soils, regardless of particle size or gradation, are primarily controlled by frictional interactions; therefore, rigid separation between sands and gravels can be misleading as it places undue emphasis on an arbitrary particle size threshold. Studies on gravelly soils can shed light on the effects of particle size and gradation of coarse-grained soils if the studies track and account for the influence of key physical parameters such as C_u, particle shape, and minerology, in addition to particle size.

The dynamic response of coarse-grained soils has been investigated via undrained cyclic element testing, often using gravel-sized particles and specialized large-scale equipment to avoid adverse boundary conditions. Based on triaxial testing of gap-graded mixtures, Evans and Zhou (1994) concluded that cyclic strength decreases with increasing gravel content. In contrast, Kokusho et al. (2004) concluded that cyclic strength was insensitive to gravel content based on triaxial testing of well-graded soils sharing the same effective particle diameter (D_{10}) but different C_u values. However, Kokusho et al. (2004) did find that postliquefaction monotonic strengths increased with C_u for soils of low crushing potential. Based on large-scale direct simple shear (DSS) testing of gap-graded mixtures, Hubler (2017), Hubler et al. (2018) concluded that the effect of gravel content on liquefaction potential and dynamic response varies with state properties (e.g., D_R, σ'_v) and loading conditions [e.g., applied cyclic stress ratio (CSR)]. The test matrix of these previous studies has provided useful insights; however, it is challenging to aggregate the data sets and draw more quantitative conclusions that can lead to generalized guidance at the field scale.

[1]Design Engineer, Division of Safety of Dams, Dept. of Water Resources, 2720 Gateway Oaks Blvd., Sacramento, CA 95833. Email: alexander.pires-sturm@water.ca.gov

[2]Professor, Dept. of Civil and Environmental Engineering, Univ. of California, Davis, One Shields Ave., Davis, CA 95616 (corresponding author). ORCID: https://orcid.org/0000-0002-9809-955X. Email: jdejong@ucdavis.edu

Note. This manuscript was submitted on January 15, 2021; approved on January 25, 2022; published online on April 14, 2022. Discussion period open until September 14, 2022; separate discussions must be submitted for individual papers. This paper is part of the ***Journal of Geotechnical and Geoenvironmental Engineering***, © ASCE, ISSN 1090-0241.

Liquefaction of soils exhibiting a wide range of D_{50} and C_u values has been observed in the field and documented in literature (e.g., Andrus and Youd 1987; Towhata et al. 2014; Cubrinovski et al. 2017). These soils have a permeability low enough to generate excess pore pressures during cyclic loading, and yet many classify as well-graded gravelly soils, which is expected to make them stronger and stiffer than poorly graded sands. The limited number of case histories and the widely varying properties of well-graded coarse-grained soils has precluded the development of a separate industry-standard triggering curves for gravelly soils. The curves developed by Cao et al. (2013) are insightful; however, use of the nonstandard Chinese dynamic penetration test (DCPT) limits their use in broader engineering practice. Ghafghazi and DeJong (2016) performed a reanalysis of seven well-documented case histories of gravelly soil liquefaction to assess the applicability of sand-based triggering curves. Fig. 1 presents the grain size distributions of the liquefied soils included in the reanalysis. Common among the soils are their high coefficients of uniformity (C_u) and a substantial proportion of fine sands, silts, and clays, which controlled their permeability. The study concluded that it was not unreasonable to use the sand-based liquefaction triggering curves to evaluate gravelly soils. However, the study acknowledged the small data set, the lack of testing details, and the challenges associated with converting different penetration resistances to equivalent standard penetration test (SPT) $(N_1)_{60}$ values.

This paper presents the results of a parametric centrifuge study designed to elucidate the influence of particle size and gradation on liquefaction potential and dynamic response. While prior studies have investigated aspects of this topic, this study was designed to integrate and systematically study how the critical parameters of D_{50} and C_u influence the dynamic response of a uniform, level-ground deposit subjected to a sequence of shaking events of increasing magnitude. The centrifuge environment allowed for a controlled, field-scale simulation that allowed for tracking of other key input parameters such as relative density, CPT penetration resistance, peak ground acceleration (PGA), and Arias intensity (I_a). This holistic test design enabled direct mapping between soil properties, loading conditions, and system response, which had not been possible previously.

Nine soils ranging in D_{50} from 0.18 to 2.58 mm and C_u from 1.53 to 9.86 were tested over a broad range of relative density (D_R) and Arias intensity (I_a) levels. The interplay between these variables was studied to identify trends and areas most promising for future research. While this study is limited to sand-sized particles (based on USCS), the results may have implications on other coarse-grained soils, including gravelly soils, which are often encountered in alluvial and human-made deposits in practice. Large differences in liquefaction potential and dynamic response were observed over the relatively narrow range of D_{50} and C_u tested; therefore, it is expected that more coarse-grained gravelly soils, with larger D_{50} or C_u, will exhibit a response that differs from that of clean sands.

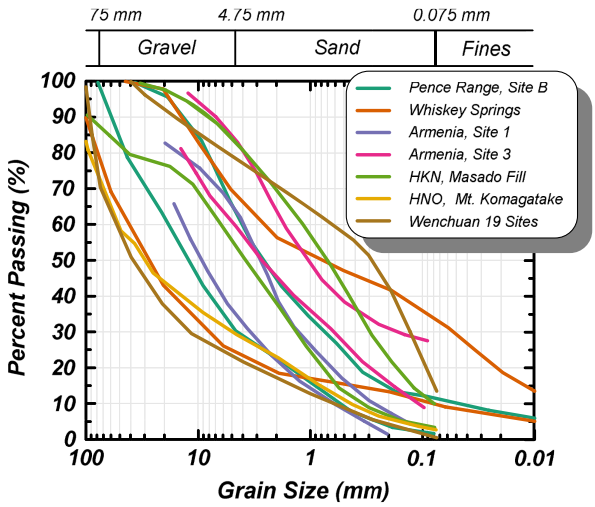

Fig. 1. Grain size distribution curves for gravelly soil liquefaction sites. (Adapted from Ghafghazi and DeJong 2016.)

Testing Program

Test Soils

Four, poorly graded soils ranging in mean grain diameter (D_{50}) from 0.18 to 2.58 mm were sourced from the Cape May Formation near Mauricetown, New Jersey. The formation is a Pleistocene, marginal-marine deposit consisting of interbedded quartzite sand and gravel containing less than 10% feldspar (Owens et al. 1998). These poorly graded soils were mined and slot sieved into poorly graded portions of the parent material with no further modifications; thus, their mineralogy and particle shape are indicative of their formation (Nichols 2009). These attributes are expected to affect liquefaction potential and dynamic response; thus, it was important to ensure they varied in a manner consistent with their naturally deposited properties. Other aspects of formation such as history and age are not relevant to this laboratory study on reconstituted soils. Henceforth these soils will be referred to via letter designation, with Soil 100A having the smallest D_{50} and Soil 100D the largest.

The poorly graded soils were combined to create five more broadly graded soil mixtures: two gap graded (85A15D, 60A40D) and three well graded (50AB, 33ABC, 25ABCD). The mixtures are named based on the percent by mass of the poorly graded soils they contain. For example, the well-graded mixture 25ABCD contains 25% by mass of poorly-graded soils 100A, 100B, 100C, and 100D. Fig. 2 presents the grain size distributions of the nine soil mixtures used in this study. The physical, index, and mechanical properties of each soil mixture were characterized via ASTM standard methods (Sturm 2019). Table 1 provides a summary of the average soil index and mechanical properties.

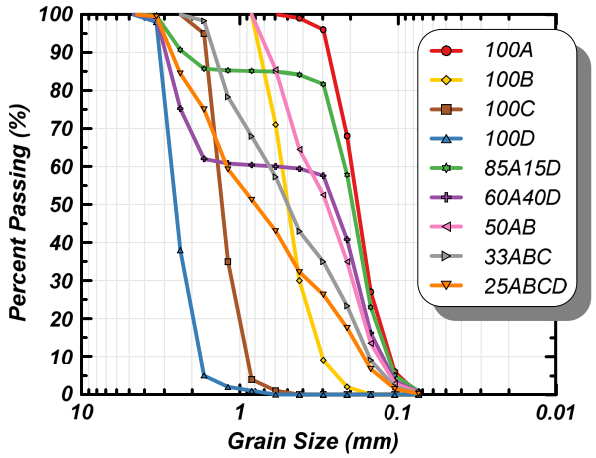

Fig. 2. Grain size distribution curves for all test soil mixtures.

Table 1. Average physical, index, and mechanical properties of the test soil mixtures

Soil	Physical properties									Index properties			Mechanical properties			
	D_{10} (mm)	D_{30} (mm)	D_{50} (mm)	D_{60} (mm)	D_{85} (mm)	D_{95} (mm)	C_u	C_c	Roundness	Sphericity	G_s	e_{max}	e_{min}	k (cm/s)	ρ_r	σ'_{yield} (MPa)	ρ_c
100A	0.12	0.15	0.18	0.20	0.27	0.30	1.68	1.02	0.69	0.79	2.62	0.881	0.579	0.017	0.014	29.3	0.469
100B	0.31	0.42	0.51	0.55	0.72	0.80	1.80	1.04	0.69	0.77	2.61	0.835	0.524	0.128	0.011	20.3	0.462
100C	0.91	1.13	1.31	1.39	1.60	1.68	1.54	1.02	0.60	0.77	2.61	0.839	0.557	1.028	0.016	11.0	0.459
100D	1.79	2.21	2.58	2.74	3.15	3.31	1.53	1.00	0.51	0.74	2.60	0.812	0.540	2.271	0.015	5.7	0.458
85A15D	0.12	0.16	0.20	0.22	1.71	2.85	1.80	1.00	0.66	0.78	2.62	0.750	0.489	0.010	0.016	31.9	0.447
60A40D	0.13	0.18	0.26	1.27	2.78	3.19	9.86	0.20	0.62	0.77	2.61	0.561	0.365	0.007	0.022	31.0	0.391
50AB	0.13	0.20	0.29	0.38	0.60	0.76	2.82	0.76	0.69	0.78	2.61	0.753	0.468	0.015	0.018	26.3	0.452
33ABC	0.15	0.26	0.51	0.66	1.35	1.60	4.41	0.68	0.66	0.77	2.61	0.622	0.397	0.022	0.028	25.8	0.428
25ABCD	0.16	0.36	0.80	1.21	2.41	3.07	7.44	0.67	0.62	0.77	2.61	0.544	0.303	0.021	0.023	27.6	0.406

Centrifuge Tests

All testing was conducted at a centrifugal acceleration of $80g$ on the 1-m radius centrifuge at the University of California Davis Center for Geotechnical Modeling (CGM). Each model was initially prepared to a relatively loose state ($D_R \approx 50\%$) using dry pluviation techniques that minimized particle segregation. A flexible shear beam (FSB) container was used to limit boundary effects during dynamic loading; however, the results of this study suggest that the FSB container still limits the maximum, single amplitude shear strains to approximately 1.5%.

The prototype site is a 9.8-m level-ground deposit that was simulated using a curved soil surface to compensate for the radial gravitational field (g-field) imposed by the centrifuge. Accelerometers (ACCs), pore pressure transducers (PPTs), and linear potentiometers (LPs) were used to measure the dynamic response of the soil column at the locations shown in Fig. 3. The models were saturated via a top-down procedure (Kutter et al. 2017) with a fluid 40 times the viscosity of water.

Each model was subjected to multiple dynamic loading events consisting of 15 uniform cycles of 1-Hz sinusoidal acceleration. The acceleration was input at the base of the model and allowed to propagate upward through the soil column. The design loading sequence consisted of 15 replicable events: 5 each at 0.1, 0.15, and $0.2g$ of peak base acceleration (PBA) followed by continued loading at variable PBA. The progressive densification caused by the dynamic loading was monitored in-flight by LPs and verified at $1g$ using hand measurements from a high accuracy Vernier depth gauge (VDG). This approach assumes uniform, one-dimensional settlement, which is a reasonable approximation based on the trends documented in Sturm (2019). Six miniature CPTs were also conducted throughout testing to study the effects of gradation on penetration resistance (Pires-Sturm and DeJong 2021).

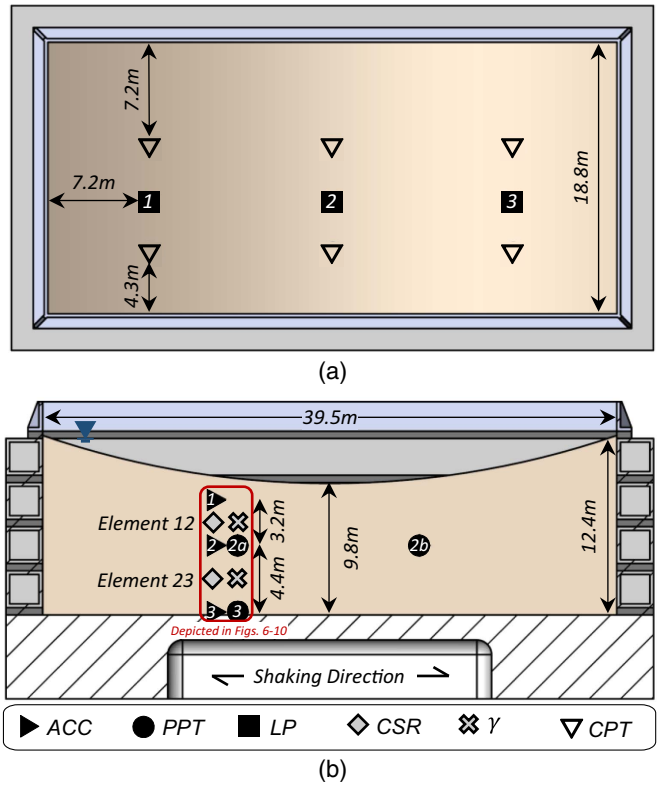

Fig. 3. Centrifuge model layout in (a) plan view; and (b) profile view.

The widely accepted procedures for centrifuge scaling outlined by Garnier et al. (2007) were followed in this study. By increasing the g-field from 1 to 80g, the vertical effective stress varied linearly with depth from zero at the ground surface to about 100 kPa at the bottom of the deposit. Using a saturation fluid of 40 times the viscosity of water within an 80-g acceleration field produces a scaling conflict between dynamic and diffusion time (Garnier et al. 2007). Because of experimental limitations, it was not practically possible to increase the fluid viscosity by 80 times; this is a common tradeoff of centrifuge testing (e.g., Kutter et al. 2017). The implications of this incongruity between g-field and fluid viscosity would cause pore pressures to dissipate faster in the model than they would in the 1-g field condition. However, based on established centrifuge protocols and past work, it was expected that excess pore pressures would reach $r_u = 1.0$ for Soil 100A (i.e., the only poorly graded sand tested herein). This expectation was confirmed during the early testing stages; therefore, scaling was appropriately calibrated to allow Soil 100A to exhibit a similar dynamic system-level response to similar liquefiable poorly graded sand in the field. The properties of the other test soils were unchanged; therefore, it is reasonable to make relative comparisons between the dynamic response across the range of C_u and D_{50} values captured in the nine soils tested. With this experimental design, it is expected that the trends present in the data accurately reflect the changes in performance that will occur in the field as a function of C_u and D_{50}, although field trends may be more complex because of phenomenon not modeled herein (e.g., layering, aging, cementation).

Additional engineering parameters were computed at Elements 12 and 23 (Fig. 4) to examine the dynamic response of the nine test soil mixtures. Time histories of shear stress (τ) were computed for each loading event using the mass-inertia summing procedure of Kamai and Boulanger (2011). The CSR was then computed by normalizing τ by the initial vertical effective stress (σ'_v) at the center of each element. Time histories of shear strain (γ) were computed for each loading event via the procedures of Brandenberg et al. (2010). Additional details regarding the means and methods used for centrifuge testing and analysis are provided in Sturm (2019).

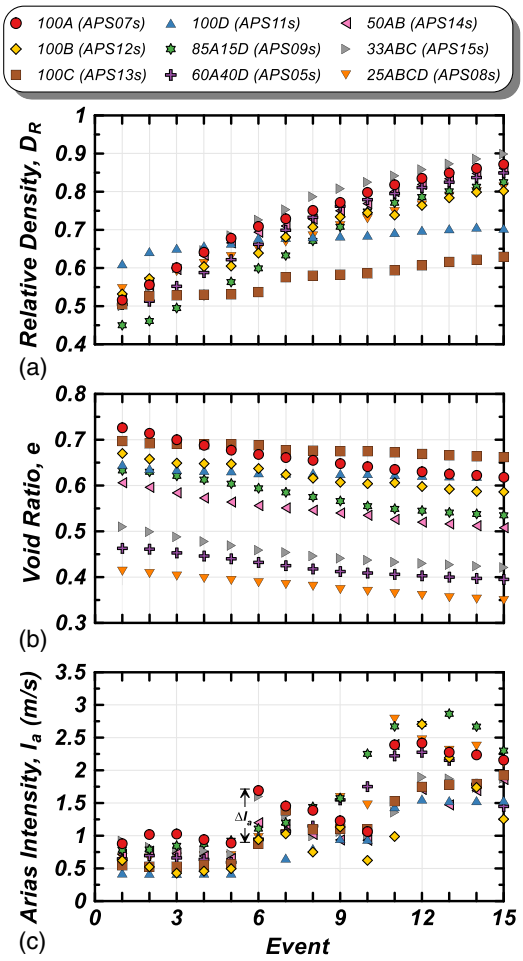

Fig. 4. Change in (a) relative density; (b) void ratio; and (c) Arias intensity with event number.

Results

To isolate the influence of particle size and gradation, all other variables should ideally be held constant and equivalent between the various models. This was practically challenging to achieve given the multitude of parameters and their variation throughout dynamic loading; therefore, the test results were scrutinized to find instances where soil capacity and the demand placed upon it were nearly constant and equivalent, as these two parameters are expected to largely dictate the soil's liquefaction potential and dynamic response. Soil capacity is represented herein by D_R because of its documented influence on cyclic strength and pervasive use in engineering practice. Fig. 4(a) illustrates the progressive increase in D_R exhibited by each soil mixture over the first 15 loading events. In general, the mixtures steadily increased from their original, as-pluviated D_R of approximately 50% to a final value of 80%–90%; however, Soils 100C and 100D reached a limit in densification due to the lack of generation of excess pore pressure. Fig. 4(b) depicts the associated decrease in void ratio for the first 15 loading events. Despite similar D_R values, the well-graded mixtures (50AB, 33ABC, 25ABCD) had much lower void ratios than the poorly graded soils (100A, 100B, 100C, 100D), with the gap-graded mixtures (85A15D, 60A40D) having intermediate values. This behavior reflects the unique $e_{\max}$ and $e_{\min}$ values (Fig. 5, Table 1) of each soil mixture, which stem from differences in their physical properties.

Arias intensity (I_a) was used to quantify the dynamic demand imparted to the models during each loading event. While PBA was used during testing, further scrutiny revealed that high-frequency accelerations, unintentionally introduced by the hydraulic actuator inducing model shaking, lead to PBA values unrepresentative of the input demand. Arias intensity was favored because its integration scheme more appropriately weighs the energy contributed by the 1-Hz component while still accounting for the influence of the high-frequency noise. The variation in I_a with event number is shown in Fig. 4(c). Overall, the target loading sequence was achieved; however, variability increases with event number and I_a because of the complex feedback mechanisms between the commanded ground motion and soil-container response.

Factors other than D_R and I_a are expected to influence the system-level dynamic response of a soil deposit. Numerous studies have concluded that prior strain history decreases the liquefaction potential of a soil deposit (e.g., Finn et al. 1970; Singh et al. 1982; Darby et al. 2019; Dobry et al. 2019); therefore, the number of loading events experienced by a model is expected to influence its dynamic response. Since each event may pose a unique demand, the cumulative (ΣI_a) serves as a metric to track the effect of loading history when comparing the dynamic response of the test soil mixtures. Furthermore, large increases in I_a may be expected to influence dynamic response: if an event is much larger than those

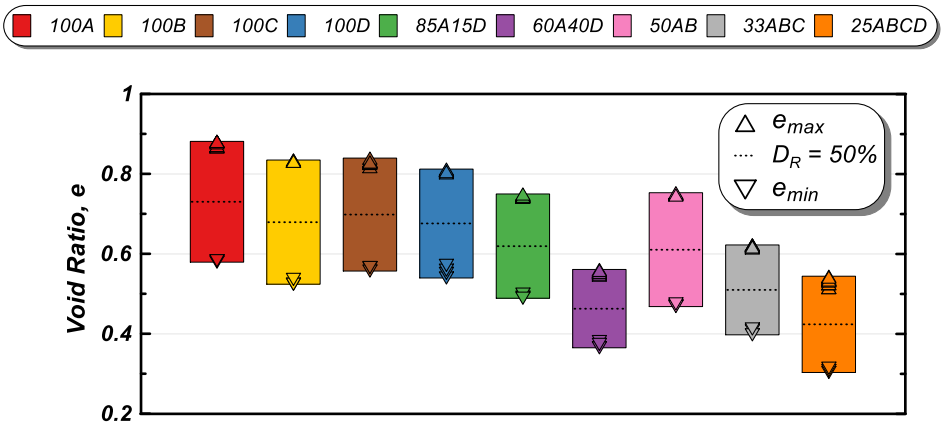

Fig. 5. Maximum and minimum void ratios of all test soils.

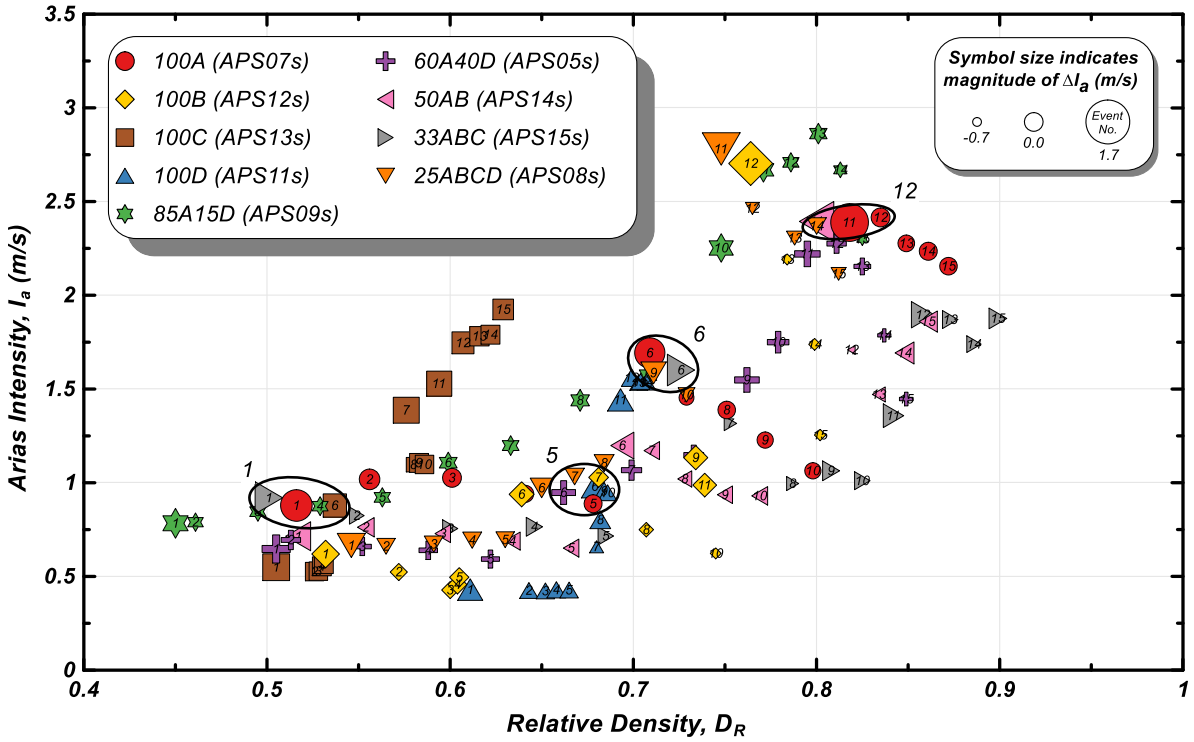

Fig. 6. Relationship between Arias intensity and relative density for the first 15 loading events.

proceeding it, the deposit will be more susceptible to liquefaction (Darby et al. 2019). This effect was tracked via the change in I_a from the proceeding event (ΔI_a). Finally, stress level is known to influence dynamic response; therefore, comparisons between the soil mixtures must be made at the same depth to isolate this effect.

The relationship between capacity (D_R) and demand (I_a) is shown in Fig. 6 for all 15 loading events applied to each model. The size of each symbol is scaled to indicate the magnitude of ΔI_a, with larger symbols indicating a larger increase in I_a compared to the proceeding event. Each symbol is also labeled with its corresponding shaking event number. Fig. 6 was scrutinized to identify clusters for analysis based on the following rank-ordered criteria:

1. Each cluster must contain Soil 100A to make comparisons to the baseline response of a clean sand.
2. Clusters should encompass a narrow range of D_R and I_a values to isolate their influence on dynamic response.
3. Clusters should encompass a narrow range of secondary influencers such as ΔI_a, event number, and ΣI_a.
4. Clusters should encompass a wide range of soil mixtures to be better elucidate the effects of gradation on liquefaction potential and system response.

Four clusters were identified in Fig. 6 and are described in Table 2: Clusters 1, 5, 6, and 12, named based on the event number corresponding to Soil 100A. Cluster 5 is presented herein whereas Clusters 1, 6, and 12 are included as Supplemental Materials.

Figs. 7–11 show the soil mixtures' dynamic response for Cluster 5. Subplots c–d and g–h present the variation in measured excess pore pressure ratio (r_u) and acceleration at middepth and the base of the model, respectively. Similarly, subplots a–b and e–f present the variation in calculated CSR and γ at Elements 12 and 23,

J. Geotech. Geoenviron. Eng., 2022, 148(6): 04022045

Table 2. Summary of clusters selected for analysis

	Cluster 1				Cluster 5					Cluster 6			Cluster 12	
Soil	100A	100C	85A15D	33ABC	100A	100B	100D	60A40D	25ABCD	100A	33ABC	25ABCD	100A	25ABCD
Test	APS07s	APS13s	APS09s	APS15s	APS07s	APS12s	APS11s	APS05s	APS08s	APS07s	APS15s	APS08s	APS07s	APS08s
Event	1	6	4	1	5	7	10	6	7	6	6	9	12	14
D_R (%)	51.6	53.7	52.9	50.1	67.8	68.1	68.6	66.2	66.8	70.9	72.6	71.1	83.5	80.0
e	0.73	0.69	0.61	0.51	0.68	0.62	0.63	0.43	0.38	0.67	0.46	0.37	0.62	0.35
I_a (m/s)	0.88	0.88	0.88	0.92	0.89	1.03	0.95	0.95	1.03	1.69	1.60	1.59	2.42	2.37
ΔI_a (m/s)	0.88	0.31	0.03	0.92	−0.05	0.09	−0.01	0.36	0.06	0.80	0.89	0.48	0.03	0.06
ΣI_a (m/s)	0.88	3.60	3.29	0.92	4.75	4.49	6.48	4.18	5.39	6.44	5.58	8.08	16.38	19.47

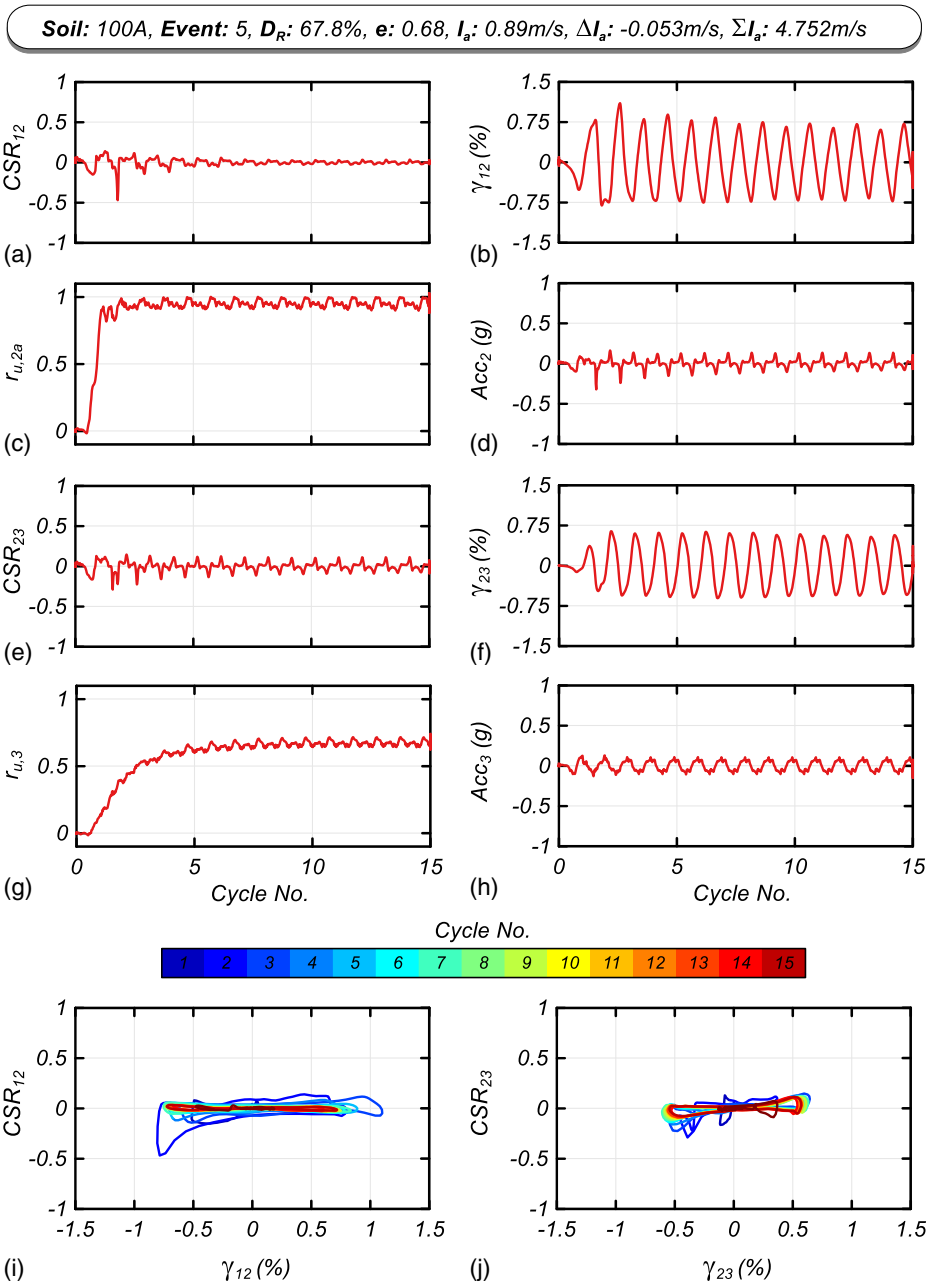

Fig. 7. Dynamic response of Soil 100A during Event 5 of Cluster 5.

respectively (Fig. 3). The relationship between CSR and γ is presented for Elements 12 and 23 in subplots i and j, respectively. Subsequently, this series of figures will be used to describe the dynamic response of each soil mixture for the clusters identified.

Cluster 5

Soil mixtures 100A, 100B, 100D, 60A40D, and 25ABCD are included in Cluster 5. Each soil mixture was at a D_R of 66%–69% when subjected to a 0.89−1.03 m/s I_a loading event. Additional

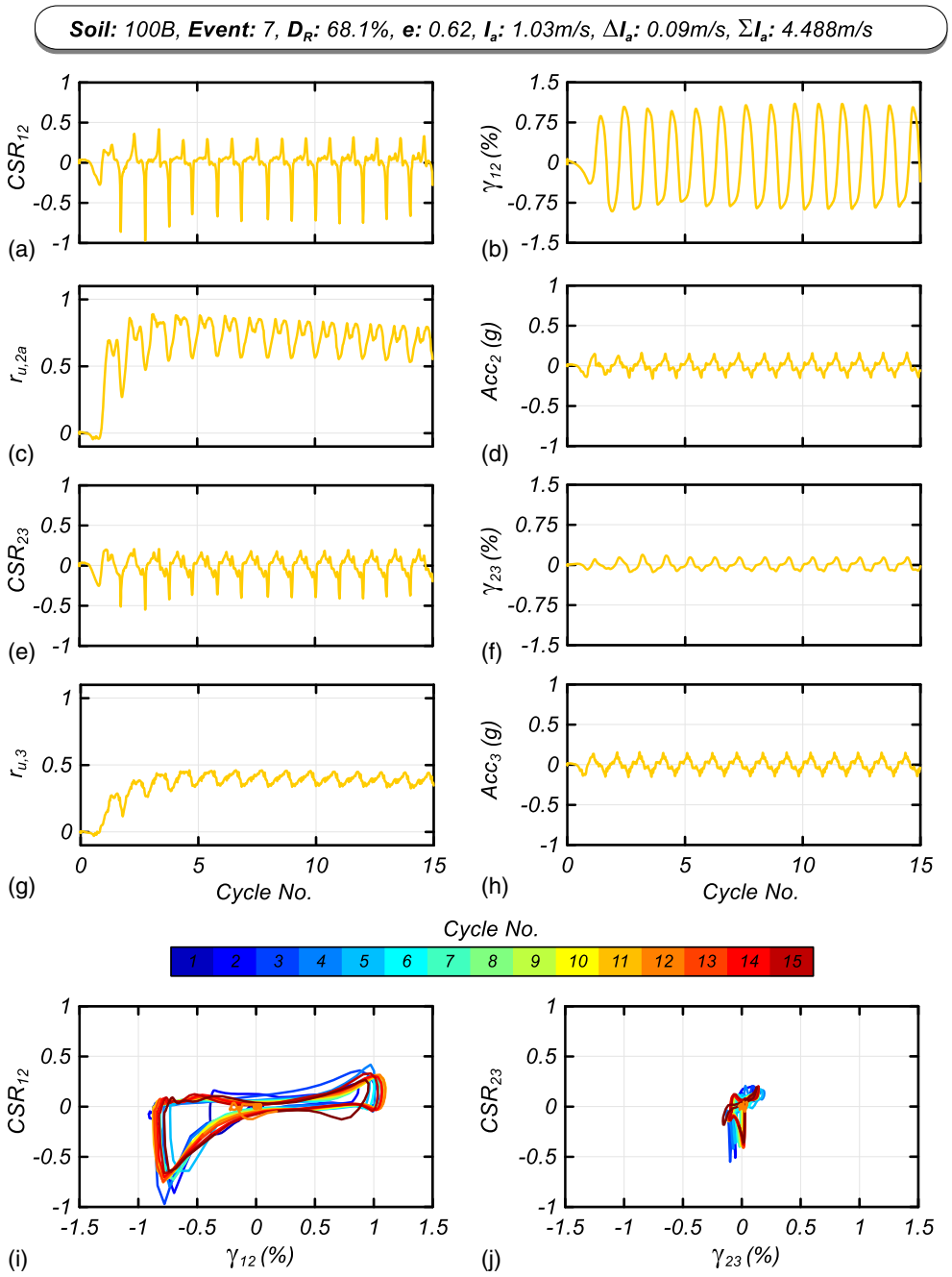

Fig. 8. Dynamic response of Soil 100B during Event 7 of Cluster 5.

information regarding event number, e, ΔI_a, and ΣI_a is provided in Table 2.

Fig. 7 presents the response of Soil 100A during Event 5. While r_u builds rapidly at middepth, initiating liquefaction in about two cycles, r_u at the model base only reaches a maximum value of 0.74. This r_u gradient leads to increasing stiffness with depth; therefore, higher CSR and lower γ values are observed at Element 12 than Element 23. Base isolation occurs near middepth after the initiation of liquefaction, which causes a reduction in CSR after Cycle 2. The increased stiffness prior to load reversal seen in Fig. 7(j) is consistent with low-level dilation.

Fig. 8 presents the response of Soil 100B during Event 7. Near the base of the model, the soil behaves as a rigid body, as exhibited by the small strain level and low pore pressures (note that this is a qualitative descriptor to describe general behaviors and does not correspond to a threshold strain level). Near middepth, a liquefied condition is suggested by the uniform shear strains of approximately 1%. Lacking a PPT at the same depth as Element 12, the liquefied condition cannot be confirmed. Unique to the response of Soil 100B are the large magnitude decreases in r_u, which coincide with the short-duration, high-amplitude CSR spikes near middepth. While this behavior is typically associated with dilation, the r_u drops are larger in magnitude (approximately 0.35) than those observed in other soils and may be indicative of simultaneous pore pressure dissipation in the higher-permeability soil. Overall, the decreases in pore pressure result in temporary increases in stiffness, which limit shear strains despite moderate CSR levels.

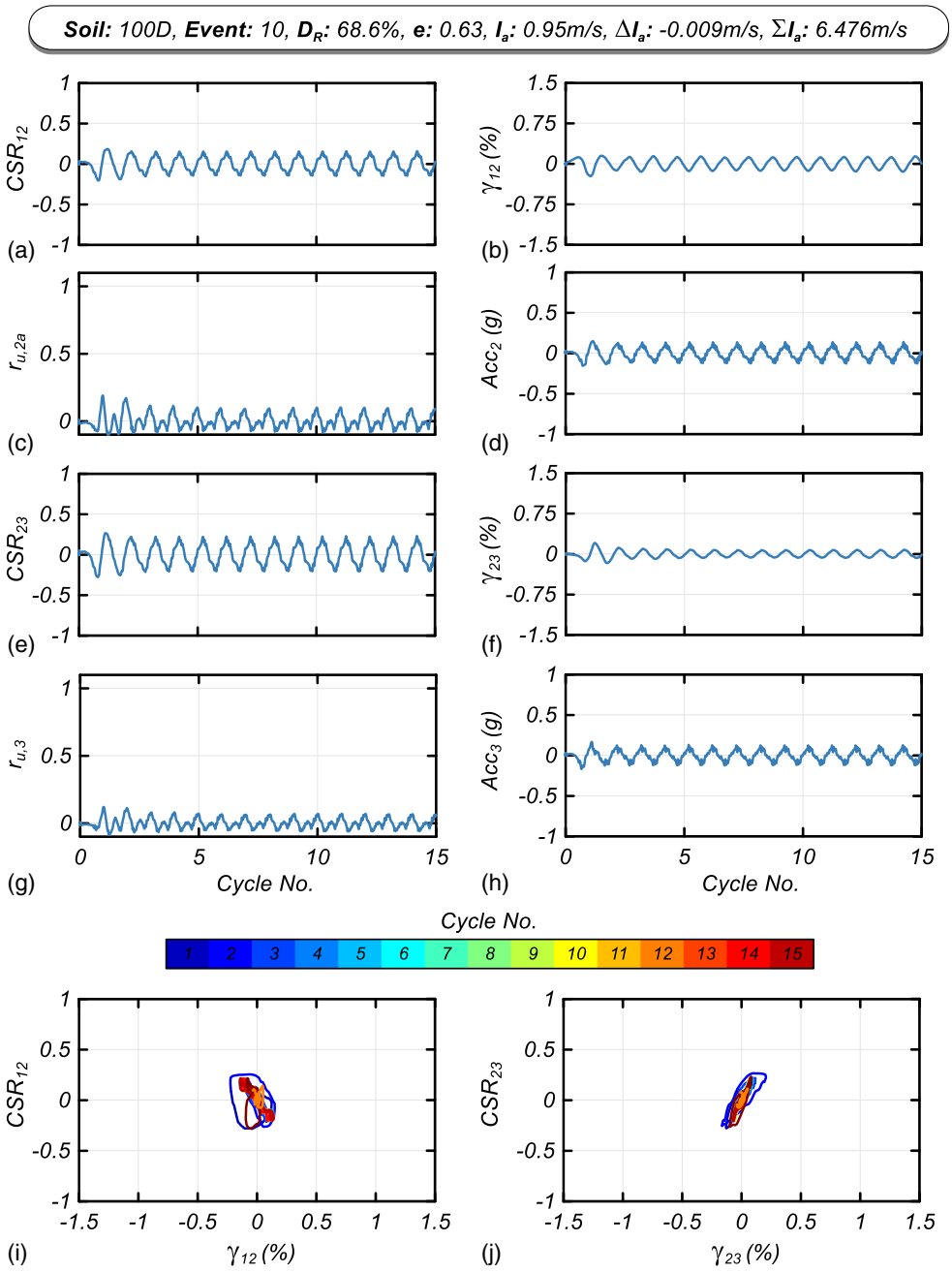

Fig. 9. Dynamic response of Soil 100D during Event 10 of Cluster 5.

Fig. 9 presents the response of Soil 100D during Event 10. Liquefaction is not initiated at any point with a peak r_u value of 0.2 observed at middepth. Because the high permeability prevents excess pore pressure generation, the entire column exhibits a rigid response.

Fig. 10 presents the response of Soil 60A40D during Event 6. Excess pore pressure builds gradually with each cycle at middepth and the base of the model; however, neither is high enough to constitute liquefaction. The r_u gradient with depth and high shear strains strongly suggest that liquefaction was initiated in the first few cycles at Element 12 (though a PPT was not present to confirm this hypothesis). As seen in Fig. 10(i), shear strains continue to grow with each postliquefaction loading cycle (cyclic mobility) (Idriss and Boulanger 2008). Furthermore, the spikes in CSR observed at Element 12 are the largest observed thus far and indicate enhanced dilation. The response near the model base is markedly different: the soil behaves as a rigid body at Element 23 because of the small r_u values.

Fig. 11 presents the response of Soil 25ABCD during Event 7. A malfunction in PPT_3 prevented the measurement of r_u at the base of the model; however, the relatively high γ values observed at Elements 12 and 23, as well as the rapid generation of r_u at middepth, suggest uniform liquefaction in approximately three cycles. Cyclic mobility is evident in the stress-strain response at Elements 12 and 23. Additionally, evidence of dilation is observed in both the acceleration and CSR time histories, with stronger dilation occurring at shallow depths. Overall, the dynamic response of Soil 25ABCD is similar to 60A40D; however, Soil 25ABCD exhibits enhanced dilation and a more uniform response with depth.

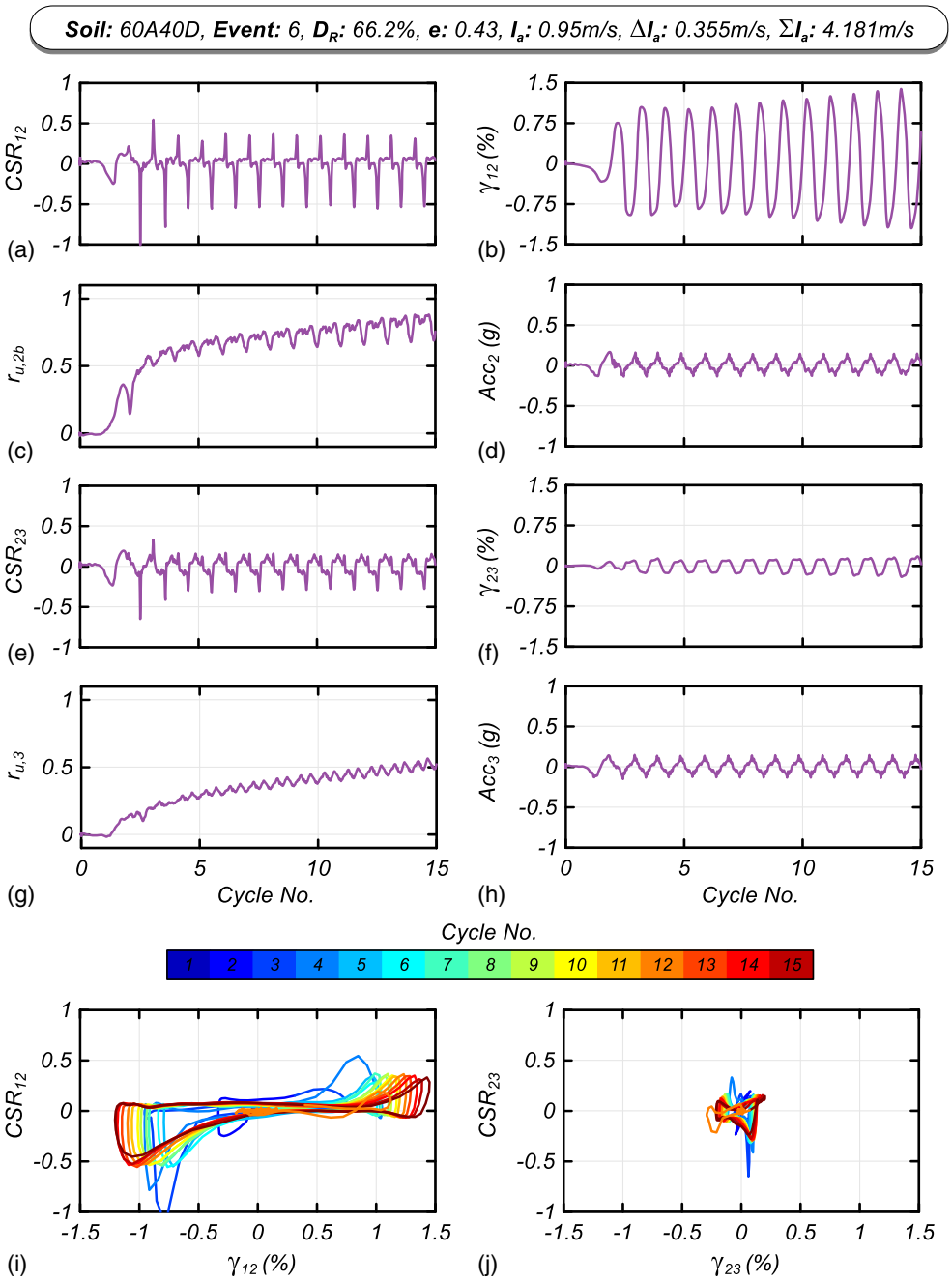

Fig. 10. Dynamic response of Soil 60A40D during Event 6 of Cluster 5.

Discussion

Soil Response

Differences in permeability (k) largely control the liquefaction potential and dynamic response exhibited by the poorly graded soils (100A, 100B, 100C, 100D). Sustained liquefaction cannot occur if pore pressures dissipate faster than are generated by the contracting soil skeleton. In centrifuge testing, the rate of pore pressure dissipation is primarily controlled by soil permeability, fluid viscosity, loading rate, and boundary conditions. Given that gradation was the only parameter varied between models, differences in soil permeability are expected to have the strongest influence on the rate of pore pressure generation and dissipation. As shown in Fig. 9, Soil 100D generated r_u peak values of 0.24; however, under comparable conditions, Soil 100A experienced rapid generation of r_u>0.95 and uniform liquefaction throughout the soil column (Fig. 6). It is hypothesized that Soil 100D did not liquefy because its permeability is 130 times greater than the permeability of Soil 100A (Table 1). Soil 100B generated peak r_u values approaching liquefaction despite having a permeability 7.5 times greater than Soil 100A; however, these high pore pressure values were not sustained and exhibited large decreases during each unload cycle (Fig. 7). This behavior is consistent with dilation; however, given the increased permeability of Soil 100B, it is more likely that the reductions in r_u are a result of permeability-controlled pore pressure dissipation.

The similarities in pore pressure generation exhibited by the clean sand, gap, and well-graded mixtures are attributed to their similar permeability values (Table 1). Despite the presence of larger

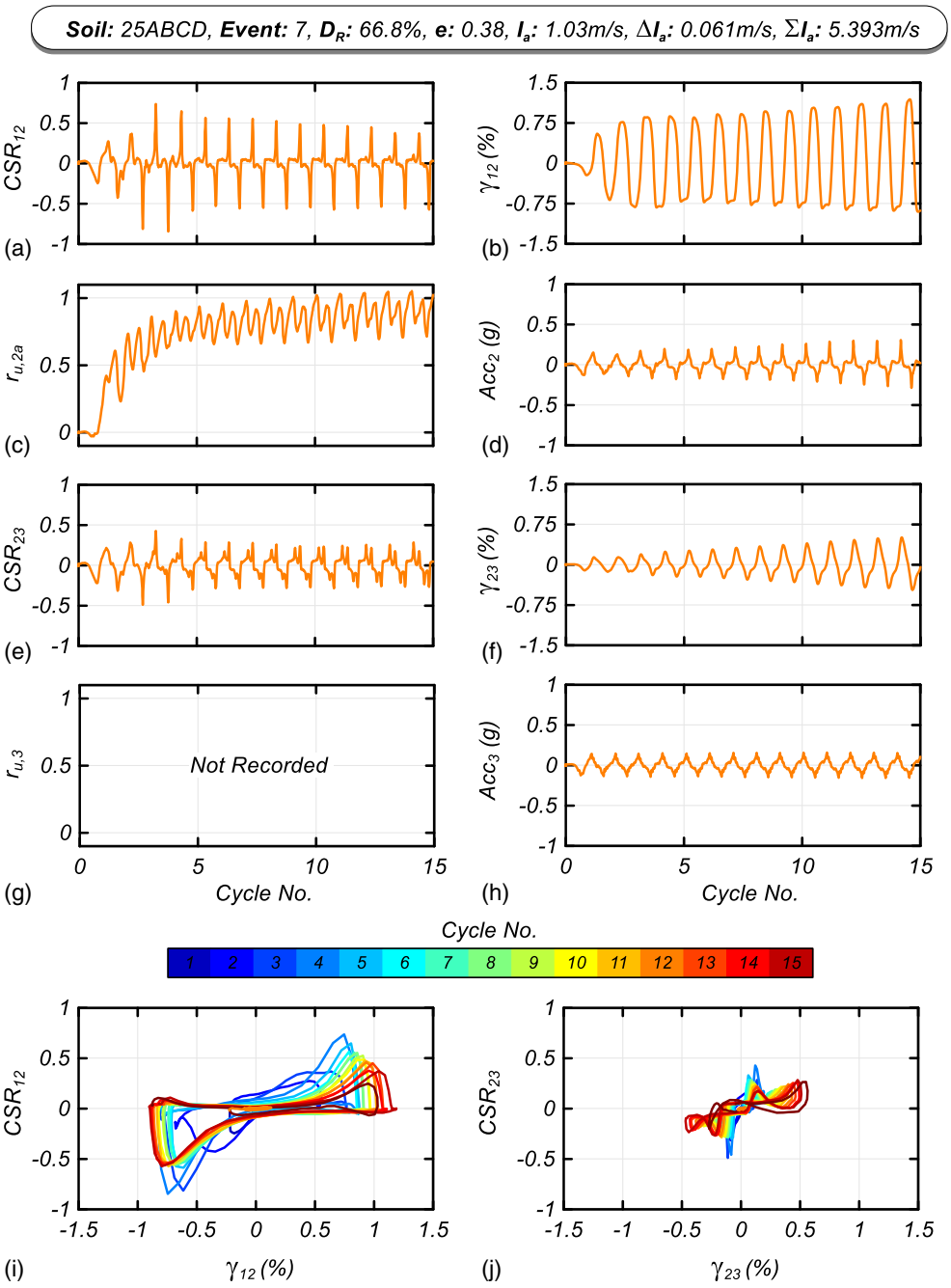

Fig. 11. Dynamic response of Soil 25ABCD during Event 7 of Cluster 5.

particles in the gap and well-graded mixtures, the permeabilities were nearly identical to Soil 100A, indicating that smaller particles (e.g., D_{10}) are the primary controlling factor (e.g., Hazen 1911).

In general, the more well-graded soils (50AB, 33ABC, 25ABCD) exhibited increased dilation compared to the clean sand (100A). Within Cluster 5, Soil 25ABCD sustains high CSR values prior to unloading as a result of dilation-induced stiffness increases, whereas Soil 100A exhibits a flat stress-strain response characteristic of poorly-graded sands (Figs. 6 and 10). Both soils reach similar maximum single-amplitude shear strains of approximately 0.5% and 0.75% at Elements 12 and 23; however, Soil 25ABCD shows evidence of cyclic mobility not observed in Soil 100A.

The dynamic response of the gap and more well-graded soils shared many similarities with respect to increased dilation. Increased dilation of the gap-graded soils is consistent with the hypothesis that dilative tendencies increase with decreasing void ratio. For the same D_R, soils 85A15D and 60A40D have lower e values than Soil 100A due to their lower e_{max} and e_{min} values (Table 1). Interestingly, the gap-graded soils tended to exhibit a variable response with depth where the upper layer (Element 12) experienced liquefaction, whereas the lower layer (Element 23) behaved as a rigid body (Fig. 9). Although this behavior was observed in other soil mixtures (e.g., Fig. 7), it was generally associated with low ΔI_a events, whereas the gap-graded mixtures exhibited a variable response with depth across a wide range of loading conditions. Differences in the behavior of gap-graded soils are often explained in the literature via compositional categorization as either matrix or clast controlled (e.g., Fragaszy et al. 1992; Evans and Zhou 1994). As demonstrated

by Hubler et al. 2017, 2018) the cyclic strength of gap-graded mixtures is not only dependent upon composition but also affected by the state properties and loading conditions. The centrifuge testing conducted herein allows for variable CSR values throughout the soil column; therefore, it is hypothesized that the binary nature of the gap-graded mixtures is a primary reason for their tendency to produce a binary response with depth. The gap-graded soils were included in this study because they are easy to conceptualize; however, their brittle sensitivity makes it difficult to generalize their behaviors. Fortunately, gap-graded deposits are seldom encountered in natural or human-made deposits; therefore, additional study may not be pragmatic.

The effects of increasing D_R, I_a, and ΔI_a manifested themselves in similar manners across all soil mixtures. Increasing D_R reduced the liquefaction potential and increased dilative tendencies in all soil mixtures aside from 100B, 100C, and 100D where permeability effects overshadowed the influence of D_R. Increased I_a placed more demand on the soil deposits, which generally lead to higher shear strains, except for cases where base isolation occurred. Overall, these effects were consistent with expectations based primarily on the testing of clean sands (e.g., Idriss and Boulanger 2008; Darby et al. 2019).

Soil Performance

Given that engineering practice is increasingly embracing performance-based design, the data presented herein was analyzed to assess the effect of particle size and gradation on system-level performance. The most appropriate measure of performance for the level-ground prototype site is volumetric strain (ε_v), computed herein based on the LP measurements at the center of the model (LP_2). The central LP was used as opposed to an average of all three LPs because it was found to be most consistent with the assumption of one-dimensional settlement. Fig. 12 shows the relationship between cumulative volumetric strain ($\Sigma\varepsilon_v$) and loading event for all nine soil mixtures. Those soils that did not liquefy (100C, 100D) experienced the least $\Sigma\varepsilon_v$, which resulted in D_R plateauing as observed in Fig. 4(a). The clean sand (100A) exhibited the greatest settlement (worst performance) with a $\Sigma\varepsilon_v$ value of approximately 8% after 15 loading events. The performance of Soil 100B was between the other poorly graded soils, likely stemming from its intermediate permeability. In contrast, the well-graded soils all exhibited lower $\Sigma\varepsilon_v$ than the clean sand, with Soil 25ABCD performing the best of the well-graded soils with a final $\Sigma\varepsilon_v$ of approximately 5%. These trends suggest that decreasing e_{max} and e_{min} values, which produced increased stiffness and enhanced dilation, translate directly to improved performance under cyclic loading. This observation explains the similar performance of Soils 25ABCD and 60A40D: despite their compositional differences, both soils share similar e_{max} and e_{min} values (Table 1), which resulted in similar $\Sigma\varepsilon_v$ trends (Fig. 11). Extending these trends to the field case suggests that well-graded soils may provide better performance than clean sands even though both can generate high r_u values due to their low permeabilities (Table 1). Future testing of alternative model geometries susceptible to large predictable deformations (e.g., embankments) may better elucidate how performance changes as the soil becomes more well graded.

System versus Element-Level Response

The centrifuge results previously discussed provide unique insights into system-level dynamic response that cannot be replicated via element-level testing. Typically, cyclic element testing mechanically imposes an undrained condition to study pore pressure generation. In contrast, the pore pressure response in centrifuge tests is primarily controlled by soil permeability and loading characteristics. This allows for pore pressure gradients with depth which can lead to pressure-driven water flow in the centrifuge model (pressure-driven flow is assumed to not occur in element tests). The loading conditions imposed during centrifuge testing are also directly controlled by soil response, with identical input ground motions leading to different CSR levels throughout the soil column. Upon initial liquefaction, the softened soil may not be able to transmit stress waves, which results in base isolation of the shallow layers. This type of behavior is not present in element testing where a constant maximum CSR is typically imposed for each loading cycle.

Cubrinovski et al. (2019) demonstrated the importance of these and other system-level responses when analyzing 55 liquefaction case histories from the 2010 to 2011 Canterbury earthquake sequence in Christchurch, New Zealand. The study concluded that accounting for system-level responses dramatically improves the

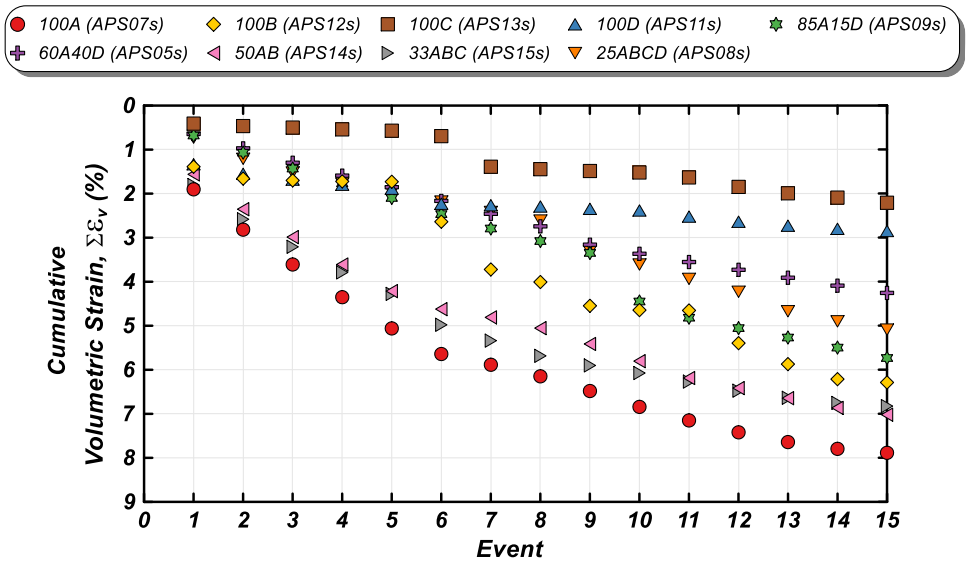

Fig. 12. Dynamic performance illustrated by change in cumulative volumetric strain with event number.

J. Geotech. Geoenviron. Eng., 2022, 148(6): 04022045

ability to explain differences in liquefaction-induced damage not captured by simplified liquefaction triggering procedures. In some instances, aspects of system-level response helped to reduce liquefaction damages (e.g., base isolation), whereas other responses worsened damages (e.g., upward flow). Although differences in stratigraphy primarily controlled the system-response of the sites analyzed by Cubrinovski et al. (2019), the paper clearly demonstrates the importance of these phenomena. Obviously, element testing is an invaluable tool to characterize the influence of particle size and gradation on dynamic response; however, the system-level response offered by centrifuge testing could be used in parallel to increase the benefit to engineering practice.

While a powerful tool, centrifuge testing has its challenges. As discussed by Kutter and Wilson (1999), changes in effective stress caused by liquefaction and subsequent dilation lead to changing shear wave velocities (V_S) throughout loading. This causes stress waves to travel at variable speeds because of the shifting site period. Though this mimics realistic field processes, it is difficult to couple stress-strain and pore pressure responses. Fig. 13 presents the results of a cyclic DSS test on Soil 100A at a D_R of 48.5% (Tognolini 2018). Liquefaction is triggered in six cycles, which leads to increased shear strains and dilation prior to unloading, as observable in both the CSR and r_u response [Fig. 12(c)]. Fig. 13(a) shows the coupled stress-strain pore pressure response, which clearly demonstrates the effect of dilation and lends itself well to additional analyses (e.g., Zhang and Wang 2012; Humire et al. 2019). In contrast, Fig. 14 presents a similar plot showing the dynamic response of Soil 100A at Element 23 during

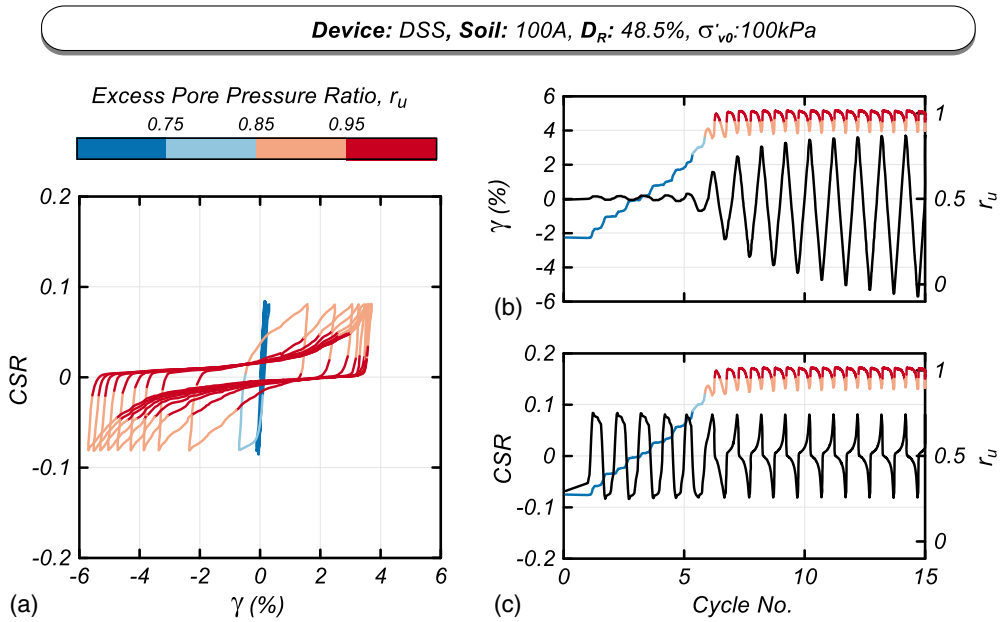

Fig. 13. Cyclic direct simple shear test results for Soil 100A.

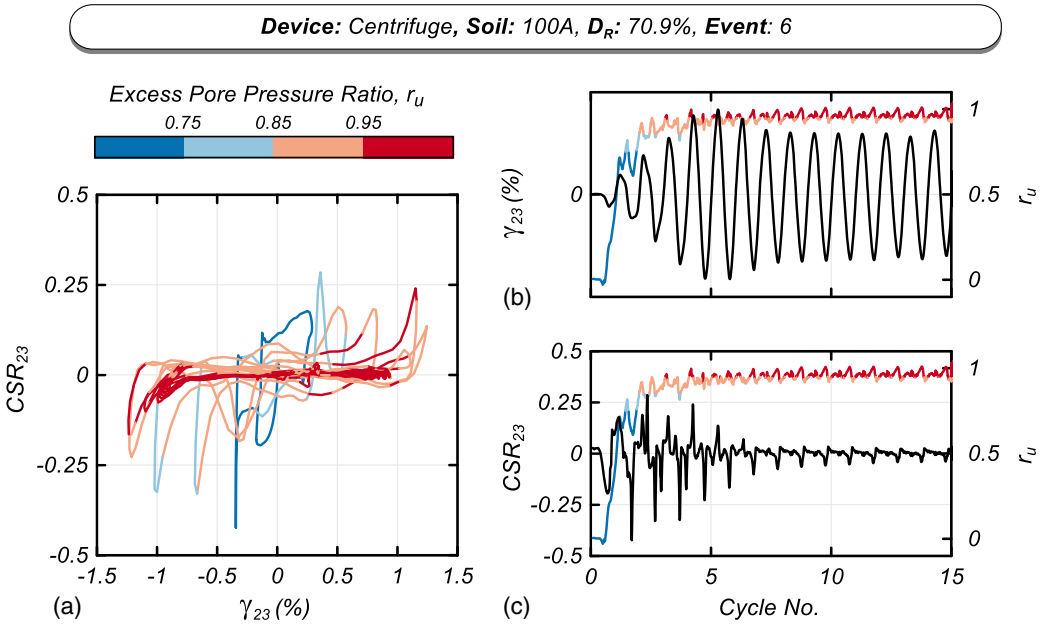

Fig. 14. Dynamic centrifuge results for Soil 100A.

Event 6 at a D_R of 70.9%. While the soil experienced dilation prior to unloading, the stress-strain and pore pressure responses are poorly correlated in time [Fig. 14(a)]. This lack of correlation stems from both the variation in site period as well as the physical distance between the PPT and Element 23. Ideally, a denser sensor array would be used to better adhere to the minimum sensor spacing recommendations of Kamai and Boulanger (2011). These challenges make it difficult to reliably assess the time of liquefaction and associated CSR, which precludes the ability to generate liquefaction triggering curves based on this data set.

Conclusions

The results of this study on the liquefaction potential and dynamic response of coarse-grained soils of varying particle size and gradation have led to the following conclusions:

- Pore pressure generation depends primarily on permeability, which is governed by particle size. At a higher permeability, poorly graded soils (100B, 100C, 100D) did not reach $r_u > 0.95$; however, the gap (85A15D, 60A40D) and more well-graded (50AB, 33ABC, 25ABCD) soil mixtures did reach $r_u > 0.95$ because their lower permeabilities prevented rapid pore pressure dissipation (Table 1). The effect of particle size on permeability has long been understood (Hazen 1911); however, the results of this field-scale simulation disprove a common misconception that gravelly soils cannot liquefy. USCS classifies a soil as gravelly based on the abundance of large grains; however, permeability is governed by the smaller grain sizes (e.g., D_{10}). As demonstrated by herein, a soil only needs to contain a smaller percentage of finer grains to reduce its permeability and enable liquefaction (defined as $r_u > 0.95$).
- Dilation during cyclic loading becomes more prominent as e_{max} and e_{min} decrease and C_u increases. For the same D_R, the gap (85A15D, 60A40D) and more well-graded (50AB, 33ABC, 25ABCD) soils had lower e values because of their decreased e_{max} and e_{min} (Table 1, Fig. 5); therefore, they exhibited enhanced dilation compared to the clean sand (100A). At the element level, the enhanced dilation results in increased stiffness before load reversal, which limited the maximum cyclic strain in the gap and more well-graded soils. For example, the maximum single-amplitude cyclic strain exhibited by 25ABCD was 1.8 times lower than Soil 100A, despite both soils reaching $r_u > 0.95$ (Figs. S5 and S7). This result demonstrates that gradation plays a key role in determining a soil's strain potential even if $r_u > 0.95$ can be sustained.
- Enhanced dilation during cyclic loading limits deformations. The clean sand (100A) experienced higher volumetric strains than any other other soil tested (Fig. 12), despite many of the soils consistently reaching $r_u > 0.95$. While this study tested sands over a narrow range of C_u values, these results imply that, as C_u increases, the susceptibility to deformations decreases relative to clean sands, all else being equal. The increase in dilative tendency with C_u has been observed in cyclic element tests (e.g., Evans and Zhou 1994; Kokusho et al. 2004; Hubler 2017); however, the results of this field-scale simulation enable these differences in elemental response to be directly related to field-scale performance.
- While the gap-graded soils (85A15D, 60A40D) exhibited many similarities to the more well-graded soils (50AB, 33ABC, 25ABCD), their brittle sensitivity made it difficult to generalize their response. Fortunately, gap-graded soils are infrequently encountered in engineering practice, as most natural soils are well-graded because of their depositional processes.
- Centrifuge testing provided insights into system-level response not replicated by element testing. The modeling of field-scale processes illustrates the interplay between soil properties, system response, and performance. Studies that combine the benefits of element and centrifuge testing may prove useful for verification of analysis procedures predicting the liquefaction potential and dynamic response.

Overall, these findings emphasize the importance of accurately characterizing and isolating the multitude of physical, index, and mechanical properties that influence liquefaction potential and dynamic response. Particle size was found to primarily influence permeability, which affects pore pressure generation and liquefaction potential. Gradation was found to primarily influence packing efficiency, which affects strain response and deformations. While this study tested sands over a relatively narrow range of D_{50} and C_u, the trends have implications for more coarse-grained soils, including gravels, which can have greater D_{50} and C_u values in natural and human-made soils. Extrapolating the trends observed herein suggests that soils with higher C_u values may be less susceptible to large deformations even if they experience liquefaction ($r_u > 0.95$).

Data Availability Statement

Some or all data, models, or code that support the findings of this study are available from the corresponding author upon reasonable request.

Acknowledgments

The authors appreciate the funding and supported provided by the National Science Foundation (#CMMI-1300518) and the California Department of Water Resources, Division of Safety of Dams. Any opinions, findings, and conclusions or recommendations expressed in this paper are those of the authors and do not necessarily reflect the views of the National Science Foundation or other agencies. This work would not have been possible without the Natural Hazards Engineering Research Infrastructure (NHERI) shared-use centrifuge facility at the University of California, Davis, funded by the National Science Foundation (#CMMI-1520581) and the support from the technical staff at the UC Davis CGM: Chad Justice, Anatoliy Ganchenko, Tom Kohnke, and Dan Wilson. The assistance, training, and advice provided by graduate students Brian Sawyer, Greg Shepard, Mohammad Khosravi, Trevor Carey, and Kate Darby are greatly appreciated. The authors thank undergraduate interns Diana Melendez, Evan Barnell, and Brian Morales for their assistance.

Supplemental Materials

Figs. S1–S9 and a brief discussion of the results for Clusters 1, 6, and 12 are available online in the ASCE Library (www.ascelibrary.org).

References

Andrus, R. D., and T. L. Youd. 1987. *Subsurface investigation of a liquefaction-induced lateral spread, Thousand Springs Valley, Idaho*. Miscellaneous Paper (GL-87-8). Vicksburg, MI: USACE.

Bolton, M. D., M. W. Gui, J. Garnier, J. F. Corte, G. Bagge, J. Laue, and R. Renzi. 1999. "Centrifuge cone penetration tests in sand." *Géotechnique* 49 (4): 543–552. https://doi.org/10.1680/geot.1999.49.4.543.

Brandenberg, S. J., D. W. Wilson, and M. M. Rashid. 2010. "Weighted residual numerical differentiation algorithm applied to experimental

bending moment data." *J. Geotech. Geoenviron. Eng.* 136 (6): 854–863. https://doi.org/10.1061/(ASCE)GT.1943-5606.0000277.

Cao, Z., T. L. Youd, and Z. Yuan. 2013. "Chinese dynamic penetration test for liquefaction evaluation in gravelly soils." *J. Geotech. Geoenviron. Eng.* 139 (8): 1320–1333. https://doi.org/10.1061/(ASCE)GT.1943-5606.0000857.

Cubrinovski, M., J. D. Bray, C. De La Torre, M. J. Olsen, B. A. Bradley, G. Chiaro, E. Stocks, and L. Wotherspoon. 2017. "Liquefaction effects and associated damages observed at the Wellington CentrePort from the 2016 Kaikoura earthquake." *Bull. N. Z. Soc. Earthquake Eng. Earthquake Eng.* 50 (2): 152–173. https://doi.org/10.5459/bnzsee.50.2.152-173.

Cubrinovski, M., A. Rhodes, N. Ntritsos, and S. Van Ballegooy. 2019. "System response of liquefiable deposits." *Soil Dyn. Earthquake Eng.* 124 (Sep): 212–229. https://doi.org/10.1016/j.soildyn.2018.05.013.

Daniel, C. R., J. A. Howie, and R. G. Campanella. 2004. "Characterization of SPT grain size effects in gravels." In *Proc., 2nd Int. Conf. on Site Characterization (ISC'2)*. Rotterdam, Netherlands: MillPress.

Darby, K. M., R. W. Boulanger, J. T. DeJong, and J. D. Bronner. 2019. "Progressive changes in liquefaction and cone penetration resistance across multiple shaking events in centrifuge tests." *J. Geotech. Geoenviron. Eng.* 145 (3): 04018112. https://doi.org/10.1061/(ASCE)GT.1943-5606.0001995.

DeJong, J. T., M. Ghafghazi, A. P. Sturm, D. W. Wilson, J. den Dulk, R. J. Armstrong, A. Perez, and C. A. Davis. 2017. "Instrumented Becker penetration test I: Equipment, operation, and performance." *J. Geotech. Geoenviron. Eng.* 143 (9): 04017062. https://doi.org/10.1061/(ASCE)GT.1943-5606.0001717.

Dobry, R., S. Thevanayagam, W. El-Sekelly, T. Abdoun, and Q. Huang. 2019. "Large-scale modeling of preshaking effect on liquefaction resistance, shear wave velocity, and CPT tip resistance of clean sand." *J. Geotech. Geoenviron. Eng.* 145 (10): 04019065. https://doi.org/10.1061/(ASCE)GT.1943-5606.0002080.

Evans, M. D., and S. Zhou. 1994. "Liquefaction behavior of sand-gravel composites." *J. Geotech. Eng.* 121 (3): 287–298. https://doi.org/10.1061/(ASCE)0733-9410(1995)121:3(287).

Finn, W. D., P. L. Bransby, and D. J. Pickering. 1970. "Effect of strain history on liquefacton of sand." *J. Soil Mech. Found. Div.* 96 (6): 1917–1934. https://doi.org/10.1061/JSFEAQ.0001478.

Fragaszy, R. J., J. Su, F. H. Siddiqi, and C. L. Ho. 1992. "Modeling strength of sandy gravel." *J. Geotech. Eng.* 118 (6): 920–935. https://doi.org/10.1061/(ASCE)0733-9410(1992)118:6(920).

Garnier, J., C. Gaudin, S. M. Springman, P. J. Culligan, D. Goodings, D. Konig, B. Kutter, R. Phillips, M. F. Randolph, and L. Thorel. 2007. "Catalogue of scaling laws and similitude questions in geotechnical centrifuge modelling." *Int. J. Phys. Model. Geotech.* 7 (3): 1–23. https://doi.org/10.1680/ijpmg.2007.070301.

Ghafghazi, M., and J. T. Dejong. 2016. "A review of liquefaction case histories in gravelly soils using SPT based triggering curves." In *Proc., 69th Canadian Geotechnical Conf.* London: International Society for Soil Mechanics and Geotechnical Engineering.

Ghali, M., M. Chekired, and M. Karray. 2019. "A laboratory-based study correlating cone penetration test resistance to the physical parameters of uncemented sand mixtures and granular soils." *Eng. Geol.* 255 (3): 11–25. https://doi.org/10.1016/j.enggeo.2019.04.015.

Hazen, A. 1911. "Discussion of "Dams on Sand Foundations" by A. C. Koenig." *Trans. Am. Soc. Civ. Eng.* 73 (Jun): 199–203.

Hubler, J. F. 2017. "Laboratory and in-situ assessment of liquefaction of gravelly soils." Ph.D. dissertation, Dept. of Civil and Environmental Engineering, Univ. of Michigan.

Hubler, J. F., A. Athanasopoulos-Zekkos, and D. Zekkos. 2018. "Monotonic and cyclic simple shear response of gravel-sand mixtures." *Soil Dyn. Earthquake Eng.* 115 (Dec): 291–304. https://doi.org/10.1016/j.soildyn.2018.07.016.

Humire, F., K. Ziotopoulou, M. S. Basson, and A. Martinez. 2019. "Framework for tracking the accumulation of shear strains during cyclic mobility." In *Proc., 7th Int. Conf. on Earthquake Geotechnical Engineering*. London: Univ. of London.

Idriss, I. M., and R. W. Boulanger. 2008. *Soil liquefaction during earthquakes*. Oakland, CA: Earthquake Engineering Research Institute.

Kamai, R., and R. W. Boulanger. 2011. "Numerical simulations of a centrifuge test to study void-redistribution and shear localization effects." In *Proc., 8th Int. Conf. on Urban Earthquake Engineering*, 455–459. Tokyo: Tokyo Institute of Technology.

Kokusho, T., T. Hara, and R. Hiraoka. 2004. "Undrained shear strength of granular soils with different particle gradations." *J. Geotech. Geoenviron. Eng.* 130 (6): 621–629. https://doi.org/10.1061/(ASCE)1090-0241(2004)130:6(621).

Kulhawy, F. H., and P. W. Mayne. 1990. *Manual on estimating soil properties for foundation design*. Palo Alto, CA: Electric Power Research Institute.

Kutter, B., and D. Wilson. 1999. "De-liquefaction shock waves." In *Proc., 7th US-Japan Workshop on Earthquake Resistant Design of Lifeline Facilities and Countermeasures Against Soil Liquefaction, MCEER-99*, 295–310. Buffalo, NY: Multidisciplinary Center for Earthquake Engineering Research.

Kutter, B. L., et al. 2017. *LEAP UCD 2017 version 1.01 model specifications*. Berlin: Springer. https://doi.org/10.1007/978-3-030-22818-7.

Nichols, G. 2009. *Sedimentology and stratigraphy.* New York: Wiley.

Owens, J. P., P. J. Sugarman, N. F. Sohl, R. A. Parker, H. F. Houghton, R. A. Volkert, A. A. Drake, and R. C. Orndorff. 1998. *Bedrock geologic map of central and southern New Jersey.* Reston, VA: USGS.

Pires-Sturm, A. P., and J. T. DeJong. Forthcoming. "Cone penetration resistance in coarse-grained gravelly soils." *J. Geotech. Geoenviron. Eng.* 115 (Dec): 291–304. https://doi.org/10.1016/j.soildyn.2018.07.016.

Singh, S., H. Seed, and C. Chan. 1982. "Undisturbed sampling of saturated sands by freezing." *J. Geotech. Geoenviron. Eng.* 108 (2): 247–265. https://ascelibrary.org/doi/10.1061/AJGEB6.0001242.

Sturm, A. P. 2019. "On the liquefaction potential of gravelly soils: Characterization, triggering and performance." Ph.D. dissertation, Dept. of Civil and Environmental Engineering, Univ. of California, Davis.

Tognolini, J. 2018. "Direct simple shear testing of coarse-grained soil mixes." Master's thesis, Dept. of Civil and Environmental Engineering, Univ. of California, Davis.

Towhata, I., et al. 2014. "Liquefaction in the Kanto region during the 2011 off the Pacific Coast of Tohoku earthquake." *Soils Found.* 54 (4): 859–873. https://doi.org/10.1016/j.sandf.2014.06.016.

Zhang, J. M., and G. Wang. 2012. "Large post-liquefaction deformation of sand, part I: Physical mechanism, constitutive description and numerical algorithm." *Acta Geotech.* 7 (2): 69–113. https://doi.org/10.1007/s11440-011-0150-7.